Proceedings World Geothermal Congress 2015
Melbourne, Australia, 19-25 April 2015

Nonlinear Poroelastoplastic Behavior of Geothermal Rocks

Mario-César Suárez A., Fernando Samaniego V., José-Eduardo Ramírez L.M.,

Omar A. Vicencio F. and Máximo E. Fernández M.

UMSNH - Edificio B, Cd. Universitaria, 5860 Morelia, Mich., México

mcsa50@gmail.com, pexfsamaniegov01@pemex.com, jedramirezlm@gmail.com, maximo.fernandez@giz.de

Keywords: Geomechanics, plastic rocks, poroelastoplasticity, poroelasticity, elastic porosity, plastic porosity.

ABSTRACT

At present time, advanced geothermal reservoir engineering requires one to quantify and predict non-isothermal multiphase fluid flow within deformable porous rocks. Frequently, the geomechanical behavior of these rocks is nonlinear and goes into the plastic range. This non-linearity comprises inelasticity and large, permanent deformations. In order to understand the true stress-strain behavior of geothermal rocks, thermoporoelasto-plasticity specific techniques are needed. If the rocks were only poroelastic there would be no numerical limits for the values of the principal components of the stress tensor. In such idealized theoretical case, geothermal rocks will never fail. In this work, an initial investigation of the general practical aspects of the outlined problem is presented. To identify the processes involved, the flow plasticity theory is introduced and mathematical numerical models are developed and solved using finite differences and finite elements. Both models are able to analyze the geomechanical deformation of geothermal rocks subjected to a nonlinear behavior. The first model is radial and includes the fluid flow, which obeys Darcy's law, and a poroelastic analysis of the rock. The second model is 3D based on continuum mechanics and flow plasticity theory with poroelastoplastic deformations. In this case, the total stress that can be applied to geothermal rocks is physically limited by a failure stress criterion. An extended Drucker-Prager failure-yielding criterion is used to represent this limit realistically. Using available field data previously published, the 3D model was applied to compute the poroelastoplastic deformation of a salt dome located in a hybrid oil-thermal reservoir located in the southern part of the Gulf of Mexico, which is related to a deep geothermal aquifer producing hot brine at 160°C and 1284 bar that invades the oil producing wells. The model shows that the vertical deformation of the salt dome is not negligible in having an influence in the global reservoir draw-down pressure.

1. INTRODUCTION

World literature on geomechanics describes land subsidence in aquifers, petroleum and gas fields, as well as geothermal reservoirs caused by their exploitation (Wang, 2000; Bundschuh & Suárez, 2010). This phenomenon is a direct consequence of permanent and irreversible rock deformations. In Enhanced Geothermal Systems (EGS), artificial stimulation is applied to deform the rock and to increase porosity and permeability. Poroelasticity studies only the behavior of porous elastic rocks containing viscous fluids such as water, brine, gas and oil. A poroelastic rock is characterized by its effective porosity, its elastic moduli and by the physical properties of the fluid that it contains. The poroelastic rock deformation can be linear or non-linear, isothermal or non-isothermal.

On the other hand, any fluid contained in a porous rock reduces its strength. The cohesive structure of a rock is weakened by the presence of liquid. All geomechanical parameters are influenced by this cohesion and directly affected by the pressure and amount of liquid present in both pores and fractures. This is the *pore-fracture-water* effect. Rock compaction, fracturing, time dependent deformations, as well as creep and subsidence mechanisms are essentially produced by volcanic and tectonic activities, by lithostatic pressure and by fluid extraction/injection. In geothermal saturated rocks, density and wave propagation speed are increased, while strength is reduced. The main hypothesis in linear poroelasticity is that the fluids flow through a deformable porous rock whose solid skeleton can be deformed elastically. Assuming that rocks are only subjected to small deformations, Hooke's law can be applied to relate strains and stresses.

Fluid extraction in geothermal reservoirs causes the reduction of the internal pore-fracture pressure and the effective aperture of pores and fissures. Many naturally fractured systems experienced intense tectonic activity in their remote past, and their original fracturing was equally intense. However, some of the systems contain fissured zones where many fractures appear closed, as in the Los Humeros, México geothermal field (Suarez, 1998). This phenomenon was due to the fact that the rock deformation was permanent, irreversible and poroelastoplastic. The poroplasticity of geothermal rocks, can exhibit either plastic dilation produced by positive tensional stresses, or plastic contraction produced by negative compressional stresses. Both processes are mechanical and thermodynamically irreversible, yielding permanent plastic deformations that could reduce the reservoirs' storage capacity. There are other important geo-thermo-mechanical effects in geothermal and hydrocarbon reservoirs. High pressure and temperature increase ductility and lower the yield point of the rock. Therefore, high confining pressure and temperature effects induce plastic flows, producing deformations beyond the limit of elastic strain (Bundschuh & Suárez, 2010).

The present flow plasticity theory (Coussy, 2004; Chin Wu, 2005; de Souza et al, 2008) assumes that a flow rule exists that can be used to compute the plastic rock deformation. It is also assumed that the total strain in geothermal rocks can be decomposed into two parts, one of them elastic or reversible and the other one plastic or irreversible. This decomposition can be additive or multiplicative; both are useful in geothermal reservoir engineering. The additive decomposition is used for small plastic deformations with Hooke's Law applied to the elastic portion, the total strain $\boldsymbol{\varepsilon}$ is equal to the elastic strain $\boldsymbol{\varepsilon}_e$ plus the plastic strain $\boldsymbol{\varepsilon}_p$, ($\boldsymbol{\varepsilon} = \boldsymbol{\varepsilon}_e + \boldsymbol{\varepsilon}_p$). The multiplicative decomposition can be used for large plastic deformations, assuming that the deformation gradient tensor $\boldsymbol{F}$ is the product of an elastic tensor and a plastic tensor, or $\boldsymbol{F} = \boldsymbol{F}_e \cdot \boldsymbol{F}_p$. To determine the plastic portion of the total strain, a flow rule, a yield criterion and a hardening model are required in both decompositions (Lee, 1969; Coussy, 2004; Souza *et al*, 2008; Anandarajah, 2010).

If the process is non-isothermal, an extra thermal strain tensor should be considered and the total strain becomes $\boldsymbol{\varepsilon} = \boldsymbol{\varepsilon}_e + \boldsymbol{\varepsilon}_p + \boldsymbol{\varepsilon}_T$. The plastic flow rule defines the evolution of the plastic strain; the hardening law characterizes the evolution of the yield limit according to the yield criterion. The main objective of this paper is to introduce these important aspects of plasticity theory applied to a couple of isothermal poroelastoplastic examples of deformable reservoirs.

2. ELASTIC AND PLASTIC POROSITY. STRAINS AND STRESSES

In order to introduce in a logical way the main variables of poroelastoplasticity, we define first the differential relationships between porosity and rock volumes. The structural volume V_B or bulk volume is the global volume occupied by the rock, with its solid grains, pores and fractures. The differential relationships between these three volumes and the porosity, are:

$$V_B = V_f + V_S \Rightarrow dV_B = dV_f + dV_S \Rightarrow 1 = \frac{dV_f}{dV_B} + \frac{dV_S}{dV_B} = \varphi + \varphi_S \tag{1}$$

where V_B, V_f, V_S, φ *and* φ_S are bulk, pore and solid volumes, fraction of the pores or porosity and fraction of the solid grains, respectively. We assume that the pores are all interconnected and completely saturated with fluid, and therefore the pore volume is equal to the fluid volume V_f. Poroelastoplasticity produces irreversible and permanent changes in porosity and in the fluid mass content inside the rock, which is defined as:

$$m_f = \frac{M_f}{V_B} = \frac{M_f V_f}{V_B V_f} = \frac{M_f \varphi}{V_f} = \rho_f \varphi \qquad \left[\frac{kg}{m^3}\right] \tag{2}$$

where m_f, M_f, ρ_f are fluid mass content, fluid mass, and fluid density, respectively. The two main variables that characterize poroplasticity are the plastic porosity φ_p and the plastic strains ε_{pij}. The fundamental poroplastic theory, assumes that plastic deformations occur instantaneously in response to increments or decrements of some specific stress σ_{ij} and fluid pressure p (Coussy, 2004). Assuming that the strain decomposition is additive, the corresponding differential relationships between these variables are:

$$\begin{aligned} &d\varepsilon_{ij} = d\varepsilon_{e\,ij} + d\varepsilon_{p\,ij},\ d\varphi = d\varphi_e + d\varphi_p \ \Rightarrow\ \varepsilon_{ij} = \varepsilon_{e\,ij} + \varepsilon_{p\,ij},\ \varphi - \varphi_0 = \varphi_e + \varphi_p \\ &\text{where: } \varepsilon_{ij} = \frac{1}{2}\left(\frac{\partial u_i}{\partial x_j} + \frac{\partial u_j}{\partial x_i}\right),\quad \varepsilon_B = \varepsilon_{11} + \varepsilon_{22} + \varepsilon_{33},\quad \varepsilon_{ii} = \frac{\partial u_i}{\partial x_i};\quad i,j = 1,2,3 \end{aligned} \tag{3}$$

Where ε_{ij}, ε_{eij}, ε_{pij},, φ_e, φ_p, φ_0 are total, elastic and plastic strains, elastic, plastic and initial porosities, respectively; $\boldsymbol{u} = (u_1, u_2, u_3)$ is the vector displacement of the solid particles in a cartesian reference basis $\{\mathbf{e}_i,\ i = 1, 2, 3\}$ and ε_B is the volumetric strain. The variables ε_{eij} and φ_e are elastic or reversible, while ε_{pij} and φ_p are plastic and irreversible variables in the poroelastoplastic non-linear process. The plastic porosity should be interpreted as the irreversible change of the porous volume.

2.1 Thermoporoelastic Equations for Hookean Rocks

In this paper we are introducing only isothermal examples based on the isothermal plasticity flow theory. The thermoporoelastic theory can be treated separately because of the additive decomposition of the total strains: ($\boldsymbol{\varepsilon}_e = \boldsymbol{\varepsilon} - \boldsymbol{\varepsilon}_p$). A full treatment of thermo-poroelasticity can be found in Coussy (2004) and, for geothermal processes, in Bundschuh and Suárez, (2010).

The equations of linear non-isothermal porous rocks relating stresses and deformations are formed by two parts; one for the skeleton:

$$\sigma_{ij} = \left(\lambda\,\varepsilon_B - b\left(p - p_0\right) - K_B\,\gamma_B\left(T - T_0\right)\right)\delta_{ij} + 2G\,\varepsilon_{ij};\quad i,j = 1,2,3 \tag{4}$$

And another one for the fluid inside the pores and fractures (Bundschuh & Suárez, 2010):

$$p = p_0 + M\left(\zeta - \zeta_0\right) - C\,\varepsilon_B - M\varphi\,\gamma_m\left(T - T_0\right) \Leftrightarrow \zeta = \zeta_0 + b\,\varepsilon_B + \frac{p - p_0}{M} + \varphi\,\gamma_m\left(T - T_0\right) \tag{5}$$

where σ_{ij}, λ, b, K_B, γ_B, T, G, are stresses, Lamé modulus, Biot-Willis coefficient, bulk modulus, bulk thermal expansivity, temperature and shear modulus, respectively. The term p_0 is the initial pressure, and T_0 is the initial temperature; δ_{ij} is the unit tensor. In equation (5) M, C, ζ, γ_m, are the two Biot moduli, the variation of the fluid content, and the thermal expansion of the fluid mass content, respectively. The right part of equation (5) is the operational definition of ζ, the main poroelastic variable in the linear theory of Biot (1972). The mathematical definitions of all these coefficients are as follows:

$$b = 1 - \frac{K_B}{K_S},\quad \frac{1}{M} = \left(\frac{\partial \zeta}{\partial p}\right)_{\varepsilon_B},\quad C = b\,M,\quad \gamma_B = \frac{1}{V_B}\left(\frac{\partial V_B}{\partial T}\right)_{p_k},\quad \gamma_m = \frac{1}{m_f}\left(\frac{\partial m_f}{\partial T}\right)_p \tag{6}$$

where K_S is the solid bulk modulus and p_k is the confining lithostatic pressure. The coefficient M is the inverse of the constrained specific storage, measured at constant volumetric strain; this parameter characterizes the elastic properties of the fluid because it measures how the fluid pressure changes when ζ changes. The coefficient C represents the coupling of deformations between the solid grains and the fluid. These three parameters b, M and C are the experimental core of the poroelastic equations.

3. THE ELASTOPLASTIC EQUATIONS. A FLOW RULE AND A HARDENING MODEL

Using full tensor notation for the strains, the general, additive elastoplastic model is:

$$\boldsymbol{\varepsilon} = \boldsymbol{\varepsilon}_e + \boldsymbol{\varepsilon}_p \;\Rightarrow\; \boldsymbol{\varepsilon}_e = \boldsymbol{\varepsilon} - \boldsymbol{\varepsilon}_p \;\Leftrightarrow\; \dot{\boldsymbol{\varepsilon}}_e(t) = \dot{\boldsymbol{\varepsilon}}(t) - \dot{\boldsymbol{\varepsilon}}_p(t), \text{ and } \boldsymbol{\varepsilon}(t_0) = \boldsymbol{\varepsilon}_0 \tag{7}$$

The point above the strains means time derivative and the last term in equation (7) is an initial condition for the total strain. It is assumed that the elastic strain tensor $\boldsymbol{\varepsilon}_e$ is computed with Hooke's law and therefore the only unknown is the plastic strain tensor $\boldsymbol{\varepsilon}_p$; its calculation solves the elastoplastic problem. The non-isothermal elastic part can be solved as indicated in subsection 2.1.

Let ψ be the free energy potential, which is assumed to be a function of the strains and of a set of internal variables $\mapsto = \{\mapsto_i, i = 1, n\}$ such as the plastic porosity; the $\mapsto_i$ are called the hardening variables. It is also assumed that this potential can be decomposed into the addition of an elastic part ψ_e and a plastic part ψ_p (de Souza et al., 2008):

$$\psi(\boldsymbol{\varepsilon}_e, \boldsymbol{\varepsilon}_p, \boldsymbol{\alpha}) = \psi_e(\boldsymbol{\varepsilon}_e) + \psi_p(\boldsymbol{\alpha}) \tag{8}$$

The plastic part ψ_p describes the hardening (or softening) of the rock. We assume in this description that the geothermal rocks are linear and isotropic. Using this decomposition of the free energy potential, the general elastic law to compute the stress tensor $\boldsymbol{\sigma}$ and the hardening thermodynamical force $\boldsymbol{\tau}$ are:

$$\boldsymbol{\sigma} = \rho \frac{\partial \psi_e}{\partial \boldsymbol{\varepsilon}_e}; \quad \boldsymbol{\tau} = \rho \frac{\partial \psi_p}{\partial \boldsymbol{\alpha}} \tag{9}$$

3.1 The Plastic Domain

The plastic flow occurs when the stresses attain a critical value. In the general case, this experimental principle can be represented by a yield function or flow potential $Y(\boldsymbol{\sigma}, \boldsymbol{\tau})$, which can be positive, negative or zero. These possible values define three different domains:

$$\Omega_E = \{\, \boldsymbol{\sigma} \,|\, Y(\boldsymbol{\sigma}, \boldsymbol{\tau}) < 0 \}, \quad \Omega_P = \{\, \boldsymbol{\sigma} \,|\, Y(\boldsymbol{\sigma}, \boldsymbol{\tau}) \leq 0 \}, \quad \Omega_Y = \{\, \boldsymbol{\sigma} \,|\, Y(\boldsymbol{\sigma}, \boldsymbol{\tau}) = 0 \} \tag{10}$$

Ω_E is the elastic domain of stresses for which plastic yielding does not occur, Ω_P is the domain of plastically admissible stresses and Ω_Y is the domain of stresses for which plastic yielding can occur. The set defined by $Y(\boldsymbol{\sigma}, \boldsymbol{\tau}) > 0$ has no physical meaning and it is said that this process is impossible to occur thermodynamically.

3.2 Plastic flow rule for rocks

The next condition is the construction of a plastic flow rule that defines the equations and evolution law for the internal variables, which are associated with the dissipative function of the process. The internal variables are the plastic strains and the set $\mapsto$. The plastic flow rule postulated by de Souza (et al., 2008) is defined as follows:

$$\dot{\boldsymbol{\varepsilon}}_p = \dot{\gamma}\, \mathbf{N}(\boldsymbol{\sigma}, \boldsymbol{\tau}) \tag{11}$$

The matrix $\mathbf{N}$ is called the flow tensor and $\dot{\gamma}$ is an unknown plastic multiplier defined in the next section.

3.3 The Hardening Model

The hardening model is (Coussy, 2004; de Souza et al., 2008):

$$\dot{\boldsymbol{\tau}} = \dot{\gamma}\, \mathbf{H}(\boldsymbol{\sigma}, \boldsymbol{\tau}) \tag{12}$$

The matrix $\mathbf{H}$ is called the generalized hardening modulus which defines the evolution of the hardening variables $\mapsto_i$. Equations (11) and (12) are evolution laws that require loading/unloading criterions or conditions that determine when the evolution of plastic strains and internal variables may occur. These conditions are:

$$Y(\boldsymbol{\sigma}, \boldsymbol{\tau}) \leq 0, \quad \dot{\gamma} \geq 0, \quad \dot{\gamma}\, Y(\boldsymbol{\sigma}, \boldsymbol{\tau}) = 0 \tag{13}$$

Under plastic yielding $\dot{\gamma} \neq 0$, a complementary equation deduced from (13) implies the following consistency condition:

$$\dot{\gamma}\, \dot{Y}(\boldsymbol{\sigma}, \boldsymbol{\tau}) = 0 \;\Rightarrow\; \dot{Y}(\boldsymbol{\sigma}, \boldsymbol{\tau}) = 0 \tag{14}$$

The matrices $\mathbf{N}$ and $\mathbf{H}$ can be computed from the flow potential $Y(\boldsymbol{\sigma}, \boldsymbol{\tau})$:

$$\mathbf{N}(\boldsymbol{\sigma}, \boldsymbol{\tau}) = \frac{\partial Y}{\partial \boldsymbol{\sigma}}, \quad \mathbf{H}(\boldsymbol{\sigma}, \boldsymbol{\tau}) = -\frac{\partial Y}{\partial \boldsymbol{\tau}} \tag{15}$$

The analytical formula to compute the plastic multiplier $\dot{\gamma}$ can be obtained from differential calculus and algebra of tensors applied to previous equations (for details see de Souza et al., 2008):

$$\dot{\gamma} = \frac{\mathbf{N}:\mathbf{D}_e:\dot{\boldsymbol{\varepsilon}}}{\mathbf{N}:\mathbf{D}_e:\mathbf{N} - \mathbf{H}\cdot\dfrac{\partial^2\psi_p}{\partial\boldsymbol{\alpha}^2}\cdot\mathbf{H}} \tag{16}$$

Where matrix $\mathbf{D}_e$ is the isotropic elasticity tensor defined by the symmetric part of the gradient of the solid flow velocity $\boldsymbol{v}$. The symbol ":" represents the inner product between two tensors of the same order:

$$\mathbf{N}:\mathbf{D}_e:\dot{\boldsymbol{\varepsilon}} = n_{ij}\, d_{ij}\, \dot{\varepsilon}_{ij}\,,\ \ \mathbf{N}:\mathbf{D}_e:\mathbf{N} = n_{ij}\, d_{ij}\, n_{ij}\,,\ \ \mathbf{D}_e = \frac{1}{2}\left(\vec{\nabla}\vec{v} + \vec{\nabla}\vec{v}^{\,T}\right) = \frac{1}{2}\left(\frac{\partial v_i}{\partial x_j} + \frac{\partial v_j}{\partial x_i}\right)\vec{e}_i \otimes \vec{e}_j \tag{17}$$

The equations herein introduced correspond to the general rate-independent plasticity model.

3.4 The Drucker-Prager Yield Criterion

The Drucker-Prager (1952; reference in Coussy, 2004) yield criterion states that (de Souza et al., 2008): "*the plastic yielding begins when the second invariant I_2 of the deviatoric stress and the hydrostatic pressure p, reach a critical combination*".

The second invariant is a function of the stress deviator **s**:

$$I_2(\mathbf{s}) = \frac{\mathbf{s}:\mathbf{s}}{2} = \frac{1}{2}s_{ij}\,s_{ij}\,,\ \ \mathbf{s} = \boldsymbol{\sigma} - p\mathbf{I},\ \ s_{ij} = \sigma_{ij} - p\,\delta_{ij} \tag{18}$$

The elastoplastic numerical simulation described later in section 5, adopts the modified Drucker-Prager yielding criterion, which includes plasticity and plastic damage (Shen et al., 2012). The plastic potential Y_{DP} in the Drucker-Prager form is:

$$Y_{DP} = \sqrt{\left(\xi\,\sigma_{t0}\,tg\ \theta\right)^2 + I_2^2} - p\,tg\ \theta \tag{19}$$

Where ξ is a parameter that defines the eccentricity of the loading surface in the effective stress space; σ_{t0} is the threshold value of the tensile stress at which plastic flow initiates; θ is the dilatancy angle; I_2 is the second invariant at the compressive meridian, and p is pressure. The modified Drucker-Prager yield/failure criterion is a generalization of the classical Mohr-Coulomb criterion; it is useful to describe the stress-strain behavior of pressure dependent materials such as porous rocks.

The following creep law is adopted:

$$\dot{\bar{\varepsilon}}_{cr} = A\left(\bar{\sigma}_{cr}\right)^n t^m \tag{20}$$

Where $\dot{\bar{\varepsilon}}_{cr}$ represents equivalent creep strain rate; $\bar{\sigma}_{cr}$ represents Von Mises equivalent stress; t is the total time variable; A, n, m are specific model parameters described in section 5.

4. FIRST EXAMPLE: A GENERAL POROELASTIC ISOTHERMAL COUPLED MODEL

Chin, Raghavan and Thomas (2000), developed an isothermal coupled model to analyze oil wells with stress dependent permeability. In this section we deduce and generalize their model from the general theory introduced in previous sections; we also add a formula to compute the porosity as a function of pore pressure and the elastic deformation for small strains. This model is formed by the following scalar and tensor equations:

$$\text{4.1)}\quad \frac{D\left(\varphi\,\rho_f\right)}{Dt} + \left(\varphi\,\rho_f\right)\vec{\nabla}\cdot\vec{v}_f = 0\ \ \left(\text{fluid mass}\right)$$

$$\text{4.2)}\quad \frac{D\left(\varphi_S\,\rho_S\right)}{Dt} + \left(\varphi_S\,\rho_S\right)\vec{\nabla}\cdot\vec{v}_S = 0\ \ \left(\text{rock mass}\right)$$

$$\text{4.3)}\quad \varphi\left(\vec{v}_f - \vec{v}_S\right) = -\frac{\mathbf{K}}{\mu_f}\cdot\left(\vec{\nabla}p - \rho_f\,\vec{g}\right)\qquad \left(\text{Darcy's law referred to the rock}\right) \tag{21}$$

$$\text{4.4)}\quad \boldsymbol{\sigma} = \lambda\,\varepsilon_B\,\mathbf{I} + 2G\ \boldsymbol{\varepsilon}\qquad\qquad \left(\text{Hooke's law for the porous rock}\right)$$

$$\text{4.5)}\quad \vec{\nabla}\cdot\left(\boldsymbol{\sigma} - p\,\boldsymbol{\delta}\right) = \rho\frac{\partial^2\vec{u}}{\partial t^2} = 0\qquad \left(2^{\text{nd}}\ \text{Newton's law for rock dynamics}\right)$$

Where $D(\varphi\rho)/Dt = \partial(\varphi\rho)/\partial t + \vec{\nabla}(\varphi\rho)\cdot\vec{v}$ represents the material or total derivative of $(\varphi\rho)$, ρ_f, ρ_s, $\boldsymbol{v}_f$, $\boldsymbol{v}_s$, $\boldsymbol{K}$, μ_f, $\boldsymbol{g}$ are fluid and solid densities and velocities, absolute permeability tensor ($k_{ij}\ \mathbf{e}_i \otimes \mathbf{e}_j$), fluid viscosity, and gravity acceleration, respectively.

Assuming that the solid rock density ρ_s is constant, and that the flow velocity of the solid grains $\boldsymbol{v}_s$ is negligible or much smaller than the porosity changes, equation (4.2) can be simplified. This is also the reason why equation in (4.5) is equal to zero:

$$\frac{D\varphi_s}{Dt}+\varphi_s\vec{\nabla}\cdot\vec{v}_s=0 \;\Rightarrow\; \frac{\partial\varphi_s}{\partial t}+\varphi_s\vec{\nabla}\cdot\vec{v}_s\approx 0 \;\Rightarrow\; \vec{\nabla}\cdot\vec{v}_s=\frac{-1}{\varphi_s}\frac{\partial\varphi_s}{\partial t}=\frac{1}{1-\varphi}\frac{\partial\varphi}{\partial t}=\frac{D\varepsilon_s}{Dt}\approx\frac{\partial\varepsilon_s}{\partial t} \tag{22}$$

Subscript *s* means solid grains properties. Note that the hypothesis of negligible $\boldsymbol{v}_s$ is equivalent to assume that the total derivative *D/Dt* is the same as the traditional partial derivative. Combining the fluid mass equation (4.1) with Darcy' Law (4.3):

$$\begin{aligned}&\rho_f\,\varphi\vec{v}_f=\rho_f\,\varphi\vec{v}_s-\rho_f\frac{\mathbf{K}}{\mu_f}\cdot\left(\vec{\nabla}p-\rho_f\,\vec{g}\right) \;\Rightarrow\; \vec{\nabla}\cdot\left(\rho_f\,\varphi\vec{v}_f\right)=\vec{\nabla}\cdot\left(\rho_f\,\varphi\vec{v}_s\right)-\vec{\nabla}\cdot\left(\rho_f\frac{\mathbf{K}}{\mu_f}\cdot\left(\vec{\nabla}p-\rho_f\,\vec{g}\right)\right)\\ \Rightarrow\quad &\vec{\nabla}\cdot\left(\frac{\mathbf{K}}{\mu_f}\cdot\left(\vec{\nabla}p-\rho_f\,\vec{g}\right)\right)+\frac{1}{\rho_f}\vec{\nabla}\rho_f\cdot\frac{\mathbf{K}}{\mu_f}\cdot\left(\vec{\nabla}p-\rho_f\,\vec{g}\right)-\frac{1}{\rho_f}\vec{\nabla}\cdot\left(\rho_f\,\varphi\vec{v}_s\right)=\frac{1}{\rho_f}\frac{\partial\left(\rho_f\,\varphi\right)}{\partial t}\end{aligned} \tag{23}$$

Introducing the isothermal fluid compressibility C_f , and assuming that fluid density is only a function of pressure:

$$C_f=\frac{1}{\rho_f}\frac{\partial\rho_f}{\partial p};\;\; \rho_f=\rho_f(p) \;\Rightarrow\; \vec{\nabla}\rho_f(p)=\frac{\partial\rho_f}{\partial p}\vec{\nabla}p;\;\; \frac{\partial\rho_f}{\partial t}=\frac{\partial\rho_f}{\partial p}\frac{\partial p}{\partial t} \tag{24}$$

Combining both equations (23) and (24):

$$\begin{aligned}&\vec{\nabla}\cdot\left(\frac{\mathbf{K}}{\mu_f}\cdot\left(\vec{\nabla}p-\rho_f\,\vec{g}\right)\right)+\frac{1}{\rho_f}\frac{\partial\rho_f}{\partial p}\vec{\nabla}p\cdot\frac{\mathbf{K}}{\mu_f}\cdot\left(\vec{\nabla}p-\rho_f\,\vec{g}\right)=\frac{\varphi}{\rho_f}\frac{\partial\rho_f}{\partial p}\vec{\nabla}p\cdot\vec{v}_s+\vec{\nabla}\varphi\cdot\vec{v}_s+\varphi\vec{\nabla}\cdot\vec{v}_s+\\ &+\frac{1}{\rho_f}\frac{\partial\rho_f}{\partial p}\frac{\partial p}{\partial t}\varphi+\frac{\partial\varphi}{\partial t}=\varphi C_f\vec{\nabla}p\cdot\vec{v}_s+\vec{\nabla}\varphi\cdot\vec{v}_s+\varphi\vec{\nabla}\cdot\vec{v}_s+C_f\varphi\frac{\partial p}{\partial t}+\frac{\partial\varphi}{\partial t}\approx\frac{\partial\varphi}{\partial t}+\varphi C_f\frac{\partial p}{\partial t}+\varphi\vec{\nabla}\cdot\vec{v}_s\end{aligned} \tag{25}$$

Replacing this equation into equation (23) we obtain a practical, coupled poroelastic general model:

$$\begin{aligned}&\vec{\nabla}\cdot\left(\frac{\mathbf{K}}{\mu_f}\cdot\left(\vec{\nabla}p-\rho_f\,\vec{g}\right)\right)+C_f\vec{\nabla}p\cdot\frac{\mathbf{K}}{\mu_f}\cdot\left(\vec{\nabla}p-\rho_f\,\vec{g}\right)=\frac{D\varphi}{Dt}+\varphi C_f\frac{Dp}{Dt}+\varphi\vec{\nabla}\cdot\vec{v}_s=\\ &=\frac{D\varphi}{Dt}+\frac{\varphi}{1-\varphi}\frac{D\varphi}{Dt}+\varphi C_f\frac{Dp}{Dt}=\frac{1}{1-\varphi}\frac{D\varphi}{Dt}+\varphi C_f\frac{Dp}{Dt}=\vec{\nabla}\cdot\vec{v}_s+\varphi\,C_f\frac{Dp}{Dt}\end{aligned} \tag{26}$$

Introducing the definition of the isothermal pore compressibility C_p :

$$\varphi C_p=\frac{-1}{\varphi_s}\frac{\partial\varphi_s}{\partial p}=\frac{-1}{1-\varphi}\frac{\partial(1-\varphi)}{\partial p}=\frac{1}{1-\varphi}\frac{\partial\varphi}{\partial p} \;\Rightarrow\; \vec{\nabla}\cdot\vec{v}_s=\frac{1}{1-\varphi}\frac{\partial\varphi}{\partial p}\frac{\partial p}{\partial t}=\varphi\,C_p\frac{\partial p}{\partial t} \tag{27}$$

Therefore, the model given in equation (26) can be written in terms of both compressibilities:

$$\boxed{\vec{\nabla}\cdot\left(\frac{\mathbf{K}}{\mu_f}\cdot\left(\vec{\nabla}p-\rho_f\,\vec{g}\right)\right)+C_f\vec{\nabla}p\cdot\frac{\mathbf{K}}{\mu_f}\cdot\left(\vec{\nabla}p-\rho_f\,\vec{g}\right)=\;\varphi(p)\left(C_p+C_f\right)\frac{\partial p}{\partial t}} \tag{28}$$

If the pore compressibility C_p is assumed constant, then equation (27) can be integrated to obtain a useful formula for φ (p):

$$\varphi\,C_p=\frac{1}{1-\varphi}\frac{\partial\varphi}{\partial p} \;\Rightarrow\; \int_{\varphi_0}^{\varphi}\frac{d\varphi}{\varphi(1-\varphi)}=C_p\int_{p_0}^{p}dp=Ln\left(\frac{\varphi}{1-\varphi}\right)_{\varphi_0}^{\varphi}=Ln\left(\frac{\dfrac{\varphi}{1-\varphi}}{\dfrac{\varphi_0}{1-\varphi_0}}\right)=C_p\left(p-p_0\right) \tag{29}$$

therefore: $\dfrac{\varphi}{1-\varphi}=\dfrac{\varphi_0}{1-\varphi_0}e^{C_p(p-p_0)} \;\Rightarrow\; \boxed{\varphi(p)=\dfrac{\varphi_0\,e^{C_p(p-p_0)}}{1-\varphi_0+\varphi_0\,e^{C_p(p-p_0)}}=\dfrac{\varphi_0}{(1-\varphi_0)e^{-C_p(p-p_0)}+\varphi_0}}$

φ_0 is any reference porosity corresponding to a fluid pressure p_0.

4.1 A coupled poroelastic non-linear radial model

We consider a radial geometry as occurs in a flowing well in an isotropic porous medium. The mathematical model (21) can be simply written in terms of the radius r if all variables and functions are assumed to be functions of the radial coordinate and time.

$$C_T = \left(C_p + C_f\right) \;\Rightarrow\; \frac{k_r}{\mu_f}\left(\frac{\partial^2 p}{\partial^2 r} + \frac{1}{r}\frac{\partial p}{\partial r} + C_f\left(\frac{\partial p}{\partial r}\right)^2\right) = C_T\;\varphi(p)\;\frac{\partial p}{\partial t} \tag{30}$$

Where $p = p\,(r, t)$. Model (30) is a non-linear partial differential equation and the total compressibility C_T, the fluid viscosity μ_f and the rock permeability k_r could be considered constants or dependent on pressure. For example, if we assume that the permeability depends only on pressure, the model becomes:

$$\frac{1}{r}\frac{\partial}{\partial r}\left(\frac{k_r(p)}{\mu_f} r \frac{\partial p}{\partial r}\right) + C_f\,\frac{k_r(p)}{\mu_f}\left(\frac{\partial p}{\partial r}\right)^2 = C_T\,\varphi(p)\,\frac{\partial p}{\partial t} \tag{31}$$

The permeability as a function of pore pressure can be approximated using the empirical Pearson's formula (1976):

$$k_r\left(\varphi(p)\right) = 0.987\left(10^{\left(13.614\;\varphi(p) - 1.8126\right)}\right)\times 10^{-15} \tag{32}$$

The numerical value of the coefficient and exponents could be experimentally adapted to different types of rocks. In radial coordinates the divergence of the stress in equation (4.5) $\sigma_r\,(r, t)$ is a linear differential equation in terms of r and can be partially integrated as follows:

$$\vec{\nabla}\cdot\sigma_r = \vec{\nabla}p \;\Leftrightarrow\; \frac{\partial\sigma_r}{\partial r} + \frac{\sigma_r}{r} = \frac{\partial p(r,t_0)}{\partial r} = p_{r,t_0} \;\Leftrightarrow\; \sigma_r(r,t_0) = \frac{r_w\sigma_w}{r} + \frac{r^2 - r_w^2}{2r}\,p_{r,t_0} = E\,\varepsilon_r(r,t_0) \tag{33}$$

Where E is the Young elastic modulus of the rock in the radial direction, r_w is the wellbore radius and σ_w is the corresponding stress at the same site. This solution is valid for each fixed time t_0, and equation (31) must be numerically solved first to obtain $p\,(r, t_0)$. The elastic strain $\varepsilon_r\,(r, t_0)$ can then be computed directly using Hooke's law, as shown in the same solution (33).

In equation (22), the divergence of the rock flow velocity $v_r\,(r, t)$ is a linear differential equation of the radius r and can be partially integrated as in equation (33):

$$\vec{\nabla}\cdot\vec{v}_r = \frac{1}{r}\frac{\partial}{\partial r}(r\,v_r) = \frac{\partial v_r}{\partial r} + \frac{v_r}{r} \approx \frac{\partial\varepsilon_r(r,t_0)}{\partial t} = \varepsilon_{r,t_0} \Rightarrow\; v_r(r,t_0) = \frac{r_w\varepsilon_w}{r} + \frac{\varepsilon_{r,t_0}}{2r}\left(r^2 - r_w^2\right) \tag{34}$$

This solution is only valid for each fixed time $t = t_0$, and the elastic strain $\varepsilon_r\,(r, t_0)$ must be computed first from equation (33) to obtain a fixed value in time. ε_w is the elastic strain at the wellbore radius. This strain could also include the plastic part of the wellbore, its elastoplastic deformation and its possible collapse.

From Darcy's law (4.3), we can compute the fluid velocity using equation (34) and the numerical solution of (31):

$$v_f(r,t_0) = v_r(r,t_0) - \frac{k_r(p)}{\varphi(p)\,\mu_f}\frac{\partial\,p(r,t_0)}{\partial r} \tag{35}$$

This solution is only valid for each fixed time $t = t_0$, equations (31) and (34) must be solved first to obtain $p\,(r, t_0)$ and $v_r\,(r, t_0)$. The radial displacement $u_r\,(r, t)$ can be integrated using equation (33):

$$\varepsilon_r(r,t_0) = \frac{\partial u_r(r,t_0)}{\partial r} = \frac{r_w\sigma_w}{rE} + \frac{r^2 - r_w^2}{2rE}\,p_{r,t_0} \;\Rightarrow\; u_r(r,t_0) = u_w + \frac{r_w\sigma_w}{E}\int_{r_w}^{r}\frac{dr}{r} + \frac{p_{r,t_0}}{2E}\int_{r_w}^{r}\frac{r^2 - r_w^2}{r}\,dr$$

$$\Rightarrow\; \boxed{u_r(r,t_0) = u_w + \frac{r_w\sigma_w}{E}\,Log\left(\frac{r}{r_w}\right) + \frac{p_{r,t_0}}{2E}\left(\frac{r^2 - r_w^2}{2} - r_w^2\,Log\left(\frac{r}{r_w}\right)\right)} \tag{36}$$

Where *Log* represents the natural logarithm and u_w is the radial displacement at the wellbore that can be null or not, depending on the purpose of the model.

The order of the solutions presented in equations (21) to (36), constitutes a practical algorithm to solve the coupled poroelastoplastic problem herein introduced. The final solution itself is practical and useful in geothermal reservoir engineering.

4.1.1 Boundary and initial conditions for the radial model

The boundary and initial conditions of the model previously developed are as follows:

1. Initial radial displacement $u_r\,(r, 0) = 0$
2. Wellbore displacement $u_r\,(r = r_w, t) = 0$ (0 if well deformation is considered).
3. External boundary displacement $u_r\,(r = r_E, t) = 0$ (0 if deformation of this boundary is considered).
4. Velocities of the fluid and solid grains at $r = r_E$, $v_f = v_r = 0$ if $u_r = 0$
5. Initial fluid pressure in the reservoir $p\,(r, 0) = p_i$
6. Internal boundary at the well $\dfrac{\partial p(r_w,t)}{\partial r} = \dfrac{-q_0\,\mu_f}{2\pi k_r\, r_w\, h_0}$
7. External boundary of the reservoir $\dfrac{\partial p(r_E,t)}{\partial r} = 0$

4.2 Effects of rock poroelasticity on pressure and radial deformation in an oil reservoir

The model assumes a homogeneous and isotropic reservoir in its initial state, with variable porosity and permeability due to reservoir radial deformation. We consider constant oil rate production from one well, located at the center of a radial reservoir with uniform thickness, uniform initial properties, and fixed outer and inner boundaries. We define a poroelastic coefficient " ξ_e " as:

$$\xi_e = \frac{b}{\lambda + 2\,G} \tag{37}$$

where b is the Biot-Willis coefficient, λ is the drained Lamé coefficient and G is the drained shear modulus. For stress sensitive rocks, the solid bulk modulus is larger than the bulk modulus. The fluid does not produce shear stresses the drained shear modulus is the same as the undrained shear modulus. The drained Lamé coefficient is directly proportional to the bulk modulus, if the bulk modulus is decreased the poroelastic rock will be more pressure dependent (increasing its compressibility) and more displacement/ expansion would be expected.

Therefore for stress sensitive reservoirs the larger the poroelastic coefficient of a rock, more displacement is expected as proved by the following figures. Using the reservoir properties of Table 1, three computer runs were made using the poroelastic coefficient values shown in Table 2 for the reservoir rock. The results correspond to 150 days of oil production.

Table 1 Numerical values of Reservoir Properties

Simulator		**Reservoir Properties**	
Reservoir nodes	200	**Initial permeability (m^2)**	$4.44\ 10^{-4}$
Wellbore radius (m)	0.09	**Initial porosity**	0.23
External radius (m)	1500	**Poroelastic Coefficient (Pa^{-1})**	$9.00111\ 10^{-10}$
Initial Pressure (MPa)	50		
Rate of oil per day (m^3/d)	450	**Oil Properties**	
Reservoir Thickness	108	**Viscosity (Pa· s)**	$3.7\ 10^{-3}$
First Timestep (seconds)	1	**Compressibility(Pa^{-1})**	$1.45\ 10^{-9}$
Producing time (days)	150	**Formation Volume Factor**	1.25

Table 2. Poroelastic coefficient ξ_e (Pa^{-1})

Blue Line	$9.00111035\ 10^{-10}$
Red Line	$1.80022\ 10^{-10}$
Green Line	$9.00111\ 10^{-11}$

Figures 1 and 2 illustrate the effect that this poroelastic coefficient has on the pressure profile and on the rock radial displacement.

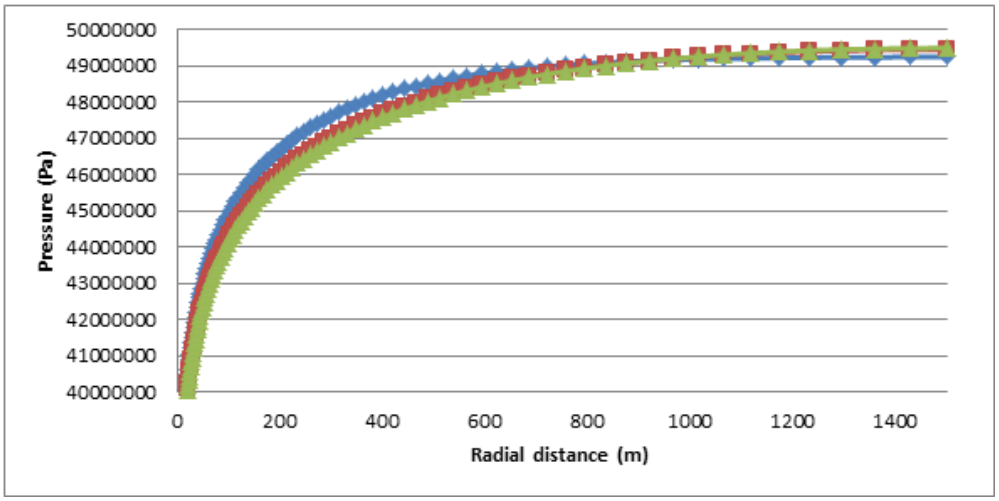


Figure 1: Effect of the poroelastic coefficient on pressure profile *p* (*r*, *t*) at a fixed time.

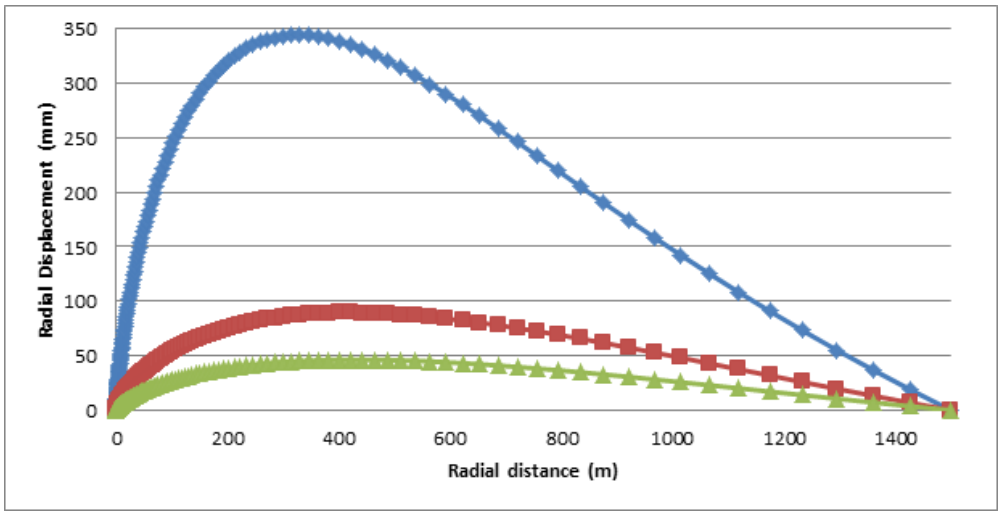


Figure 2: Effect of the poroelastic coefficient on the radial displacement u_r (*r*, *t*) at a fixed time.

4.2.1 Effect of the poroelastic properties of the seal rock on the pressure maintenance and radial displacement

Using the properties of table 1 for the reservoir rock and table 2 for the seal rock, three runs were made. Figures 3 and 4 show the obtained results.

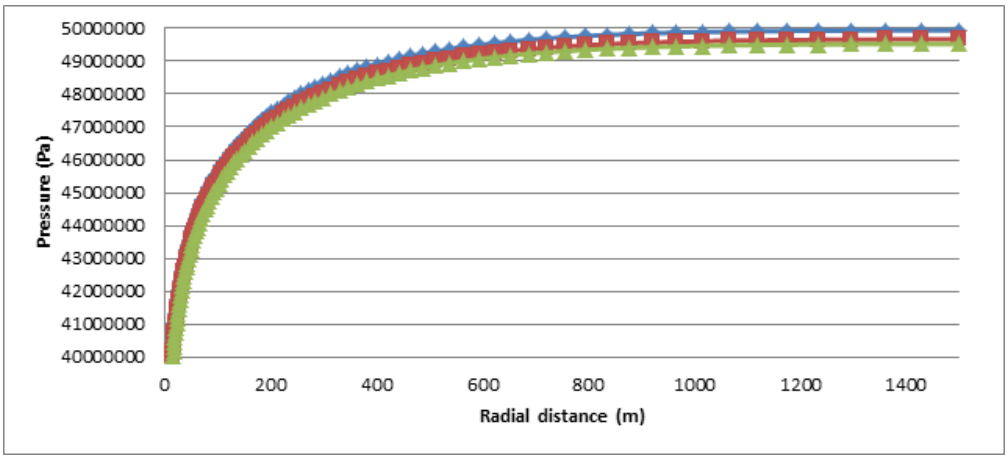


Figure 3: Effect of the seal poroelastic coefficient on the pressure profile.

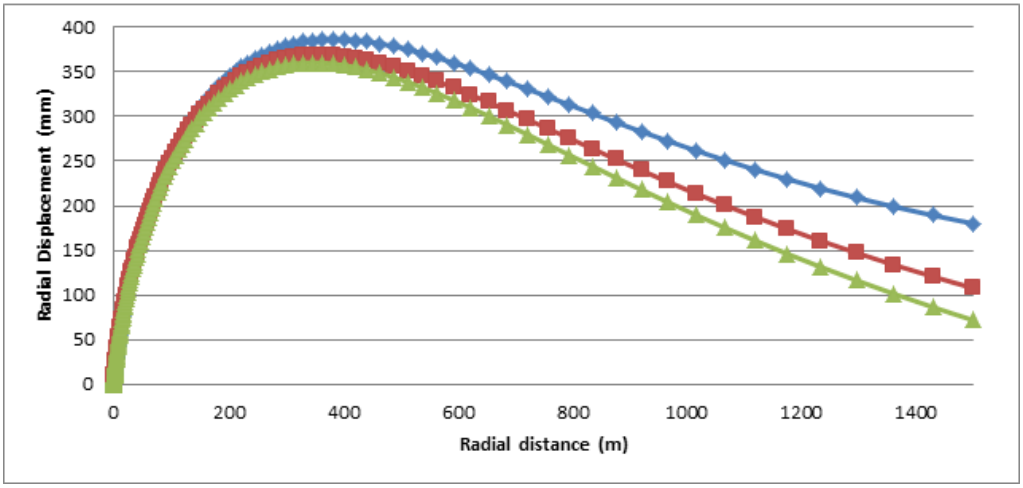


Figure 4: Effect of the seal poroelastic coefficient on radial displacement.

4.2.2 Discussion of poroelastic results

As can be seen from figures 1, 2, 3 and 4, if the poroelastic coefficient ξ_e increases, the radial displacement increases and the pressure drop decreases. For the case where the reservoir boundaries are fixed, it can be seen that at the outer boundary the pressure is larger and the radial displacement is lower. This can be explained with the aid of figure 2: because the boundaries of the reservoir rock are fixed, there is no compaction of the rock bulk volume, but there is a rock movement within the reservoir, it goes more compacted near the wellbore, reducing the porosity and permeability, but at the outer boundary the rock is expanding, and porosity and permeability are increased, this causes the pressure to be larger at the outer boundary.

For the case where the seal rock is free to move, the pressure maintenance obviously increases compared to the case where the reservoir outer boundary is fixed. The pressure profiles are different, but near the wellbore the pressure is almost the same in the three cases, they change when getting closer to the outer boundary; if the poroelastic coefficient is larger, the pressure maintenance is improved and there is a larger radial displacement.

5. SECOND EXAMPLE: APPLICATION OF THE POROELASTOPLASTIC MODEL IN 3D

5.1 Deformation of a salt dome in an oil reservoir related to a geothermal aquifer

The abnormally high concentration of dissolved salts and minerals found in samples from active wells in an oil reservoir, located in the southern part of the Gulf of Mexico at 6000 m depth, indicates the presence of solid salt domes underlying the oil reservoir. These domes are influencing the chemical composition of both oil and brine accompanying production. The extraction of hydrocarbons at this site is related to typical geothermal phenomena coupled with the active geomechanics of the salt domes. Mass migration occurs under non-isothermal conditions at different temperatures (up to 160°C) and at very high pressures (over 1284 bars). The geological system of interest is located in 1000 m water depth. Reservoir formation location is at 5000 m below sea level, location and approximated geometry of the salt dome is shown in Figure 5. The total depth of the model is 7000 m, the width is 8000 m, and the length is 8000 m. As long as this example is only made for computational purposes, it is not necessary to include a geological map of the real site. Interested readers can found a detailed description of this problem in a recently published paper (Suárez, Samaniego & Shen, 2014).

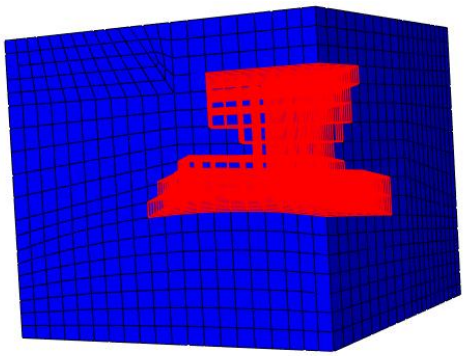


Figure 5: Position of the reservoir and the salt dome within the geological model.

To simulate the salt dome creep deformation caused by oil and brine extraction, we used the 3D model described by Shen, Bai & Standifird (2012). The model includes a visco-elasto-plastic deformation analysis and the porous fluid flow related to pressure

depletion. The model was solved using the finite element method. The numerical simulation adopts the modified Drucker-Prager yielding criterion, which includes plasticity and plastic damage that was previously discussed in section 3.

In the creep law (Eq. 20) $\dot{\bar{\varepsilon}}_{cr} = A(\bar{\sigma}_{cr})^n t^m$, the parameters are given by the following values: $A = 10^{-21.8}$; $n = 2.667$; $m = -0.2$. For the rock formation, the cohesive strength and frictional angle of the Drucker-Prager model (Shen at al., 2012) are given by the following values: $d = 1.56$ MPa, $\beta = 44°$, which correspond to values in the Mohr-Coulomb model as $c = 0.5$ MPa, $\varphi = 25°$. The values of the strength parameters for salt, adopted here by the modified Drucker-Prager model, are: $d = 4$ MPa, $\beta = 44°$, which correspond to values in the Mohr-Coulomb model as $c = 1.25$ MPa, $\varphi = 25°$.

A simplified model and four kinds of materials have been adopted, including the upper formation, the lower formation, the formation surrounding the salt, and the salt body. The corresponding parameters are listed in Table 3.

Table 3. Numerical values of material parameters

Rock setting	Density (Kg/m^3)	Young coef. (Pascal)	Poisson coef. (ad)
Top layer 1, 2, 3	2200	1.9×10^{10}	0.35
Bottom layer	2200	1.9×10^{10}	0.34
Reservoir	2200	0.9×10^{10}	0.34
Salt formation	2100	1.5×10^{10}	0.30

To keep the coupled behavior property of the model to have the least computational burden, coupled analysis for deformation and porous flow was performed for only this reservoir formation and the lower region. Other parts of the model are assumed to be non-permeable.

Pore pressure variation in the reservoir due to oil extraction goes from its original value of 82 MPa down to 70 MPa, which is a regular value of pressure drawdown. Loads applied to the model at field scale include: 1) seawater pressure and 2) self-gravity of formations and salt, which is balanced with the initial geostress. Mud-weight pressure will not appear in the field scale model. Zero-displacement constraints are applied to the four lateral sides and the bottom (Fig. 5). Oil production included in the simulation covers a period between January 1992 (5000 bpd = barrels per day), July 2004 (80,000 bpd) and December 2010 (15,000 bpd), distributed among 19 producing wells.

5.2 Numerical results of the salt dome deformation and of the pore pressure

Distribution of subsidence caused by oil extraction is shown in Figure 6. A multi-cut view is used in visualization of the vertical displacement/subsidence U3. It is seen that the maximum subsidence is 0.348 m, which occurs at the top of the reservoir.

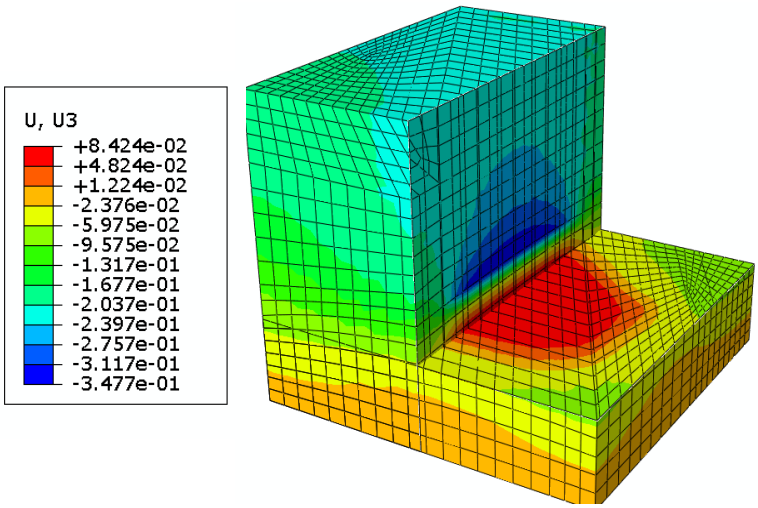


Figure 6: Contour of the vertical displacement/subsidence (U3) of the salt dome due to oil production.

Distribution of pore pressure corresponding to oil production is shown in Figure 7. A multi-cut view is used in visualization of the vertical displacement/subsidence U3. Pressure drawdown is limited to the reservoir region defined in Figure 5. Values of pore pressure are set unchanged for regions beyond the reservoir by setting very low permeability.

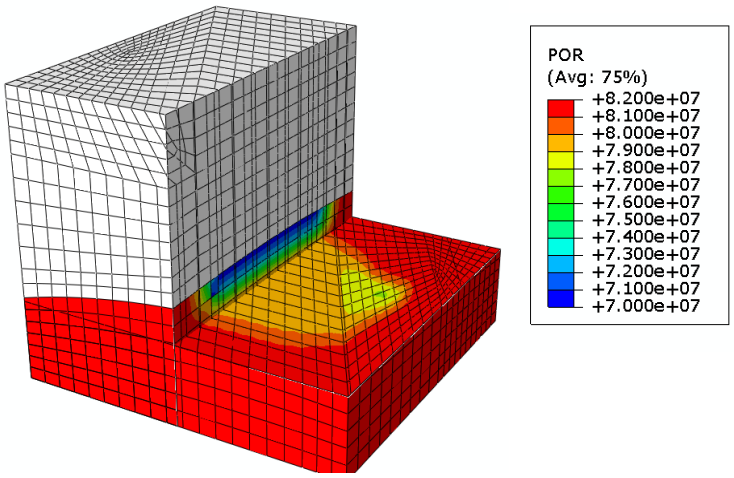


Figure 7: Contour of the pore pressure variation due to oil extraction between 1992 and 2010.

6. CONCLUSIONS

In this research paper we presented the general problem of elastoplasticity of geothermal rocks. A brief description of the general flow plastic theory was introduced and two examples of application were developed and solved. The first example covers a general poroelastic model and a simplified particular case when the system has radial geometry as occurs in a flowing well in an isotropic porous medium. Numerical results were graphically presented, showing the effect that poroelasticity has on the pressure profile and on the rock radial displacement. These results can be extended to the numerical study of well collapse.

The second example solves a three-dimensional poroelastoplastic problem, corresponding to the permanent deformation of a salt dome located in the Gulf of Mexico, which is related to an oil reservoir under exploitation. In this case, hot brine invasion occurs that involves typical geothermal phenomena coupled to the extraction of oil from the reservoir related to the salt dome. The solid salt body experiences a continuous visco-elasto-plastic deformation originated by the oil extraction and brine. The geomechanics of this deformation was modeled using the modified Drucker-Prager yield/failure criterion and finite elements. The maximum subsidence calculated is 0.348 m, which occurs at the top of the reservoir. This deformation affects the pore pressure profile and the pressure drawdown produced by the oil and brine extraction.

REFERENCES

Anandarajah, A.: Computational Methods in Elasticity and Plasticity, Springer, (2010), 633 pp.

Biot, M.A.: Theory of finite deformations of porous solids. *Indiana Univ. Math. J.* 21:7, 597–620, (1972).

Bundschuh, J. and Suárez-Arriaga, M.C. Introduction to the Numerical Modeling of Groundwater and Geothermal Systems - Fundamentals of Mass, Energy and Solute Transport in Poroelastic Rocks. Taylor & Francis Group, (2010), 479 pp.

Chin, L.Y., Raghavan, R., and Thomas, L.K.: Fully Coupled Geomechanics and Fluid-Flow Analysis of Wells with Stress - Dependent Permeability, *SPE Journal*, **5**:1, (2000), 32-45.

Coussy, O.: Poromechanics, Ed. John Wiley & Sons, Ltd (2004).

De Souza, E.A.N., Peric, D. and Owen, D.R.J.: Computational Methods for Plasticity, Wiley, (2008), 791 pp.

Lee, E. H.: Elastic-Plastic Deformation at Finite Strains.,*Journal of Applied Mechanics* **36**:1, (1969), 1-6.

Shen, X., Bai, M. and Standifird, W.: Drilling and Completion in Petroleum Engineering – Theory and numerical applications. Volume 3, Multiphysics Modeling series, Taylor & Francis Group, (2012), 233 pp.

Suárez, M.C., Samaniego, V.F., and Shen, X.: Salt domes deformation coupled to the flow of geothermal brine and oil, 14IACMAG *Proceedings*, 14th International Conference of the International Association for Computer Methods and Advances in Geomechanics, Kyoto, Japan, September 22-25, (2014).